

Ultrahigh-Resolution Optical Vector Analysis Based on Optical Single-Sideband Modulation

Shilong Pan, *Senior Member, IEEE, Member, OSA*, and Min Xue

(Invited Paper)

Abstract—Knowing magnitude, phase, and polarization responses is of great importance for fabrication and application of optical devices. A large variety of parameters such as insertion loss, dispersion, group delay, polarization-dependent loss, and polarization mode dispersion can be obtained based on these responses. Conventional approaches achieve the optical spectral responses by sweeping the wavelength of a laser source. Restricted by the low-wavelength accuracy and poor wavelength stability of the wavelength-swept laser source, the resolution of the optical vector analyzers (OVAs) are usually poor (> 1.6 pm). To achieve ultrahigh resolution measurement, an OVA based on optical single-sideband (OSSB) modulation has been proposed and developed, which potentially has a sub-Hz resolution. However, electrical-to-optical and optical-to-electrical conversions are required to implement the electrical frequency sweeping and to detect the phase and magnitude information in the electrical domain, which limits the spectral measurement range, accuracy, and dynamic range. In the past decade, great efforts have been devoted to deal with these problems. In this paper, techniques for constructing high-performance OSSB-based OVAs are discussed with an emphasis on the system architectures and operation principles for improving the spectral measurement range, accuracy, and dynamic range of the measurement system. Possible future research directions are also discussed.

Index Terms—Measurement techniques, microwave photonics, optical variables measurement, optical vector analyzers (OVAs), optical modulation.

I. INTRODUCTION

IN applications such as optical single molecule detection [1]–[3], non-Hermitian parity-time-symmetric quantum mechanics [4], slow-light-based optical storage [5], [6], on-chip optical signal processing [7], on-chip optical nonlinear effects [8], and high-precision optical sensing [9], [10], optical devices having the capability to finely manipulate the optical spectrum are highly desired, which leads to the development of a fiber Bragg grating (FBG) with a 3-dB bandwidth of 9 MHz [11], and an optical micro-resonator with a Q value of 1.7×10^{10} [12] (corresponding to a 3-dB bandwidth of 11.4 kHz if the center wavelength is 1550 nm). Knowing the spectral responses are

of great importance for the fabrication and application of these devices. Optical vector analysis is such a technology which can measure the magnitude, phase and polarization responses of optical devices and further achieve other important parameters such as insertion loss (IL), dispersion, group delay, polarization dependent loss, polarization mode dispersion and so on. Conventionally, optical vector analyzers (OVAs) are implemented based on modulation phase-shift approach [13] or interferometry approach [14], which provide large dynamic range and wide measurement range. By using multiple sidebands in different polarization states, complex dispersion can be measured in a single sweep [15], [16]. However, both approaches achieve the optical spectral responses by sweeping the wavelength of a laser source. Restricted by the low wavelength accuracy and wavelength stability of the state-of-the-art wavelength-swept laser source, the resolution of the conventional OVAs are usually larger than 1.6 pm (i.e. 200 MHz at 1550 nm) [17], which is difficult to obtain the optical spectral responses with MHz-level or less fine structures. To improve the measurement resolution, one effective approach is to apply the high-resolution spectral analysis in the electrical domain via electrical-to-optical and optical-to-electrical conversions. Two of such OVAs were proposed and developed [18]–[32].

One is realized based on optical channel estimation (OCE). In the OCE-based OVA, an orthogonal frequency division multiplexing (OFDM) signal with known symbols is generated in the electrical domain which is converted to an optical OFDM signal at an electro-optic modulator (EOM). The generated optical signal is transmitted through the optical device under test (DUT), so the optical spectral responses of the DUT in a certain frequency range are carried on the optical OFDM signal. Then, the optical OFDM signal is converted back to the electrical domain, after which the received symbols are compared with the original ones, so the optical spectral responses can be calculated [18]–[24]. The OCE-based OVA can achieve fast and high resolution measurement (e.g. 0.732-MHz resolution reported in [24]), but the dynamic range would be reduced with the frequency resolution since the electrical power is distributed to a large number of frequency components, leading to a small signal-to-noise ratio of each frequency component. In addition, the severe intermodulation distortion in the EOM restricts the maximal electrical power introduced to the EOM. As a result, the typical dynamic range is only 15 dB for a 5.86-MHz resolution [22], which is too small for characterizing most of the high-Q optical devices. Moreover, only the linear optical devices

Manuscript received June 8, 2016; revised July 30, 2016, August 3, 2016, and August 4, 2016; accepted August 4, 2016. Date of publication August 4, 2016; date of current version February 22, 2017. This work was supported in part by the National Natural Science Foundation of China (61527820, 61422108), the Jiangsu Provincial Program for High-level Talents in Six Areas (DZXX-034), and the “333 Project” of Jiangsu Province (BRA2015343).

The authors are with the Key Laboratory of Radar Imaging and Microwave Photonics, Ministry of Education, Nanjing University of Aeronautics and Astronautics, Nanjing 211106, China (e-mail: pans@ieec.org; xuemin@nuaa.edu.cn).

Color versions of one or more of the figures in this paper are available online at <http://ieeexplore.ieee.org>.

Digital Object Identifier 10.1109/JLT.2016.2598477

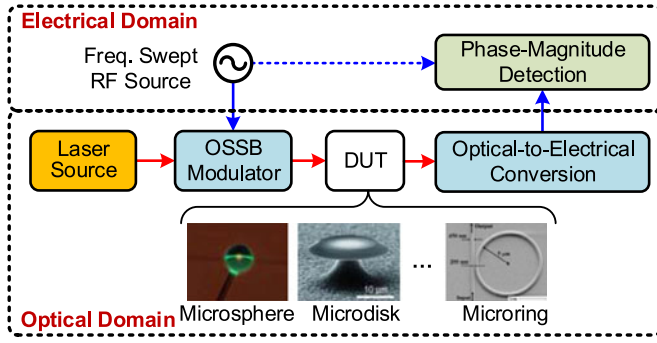


Fig. 1. Block diagram of the OSSB-based OVA. OSSB: optical single sideband; DUT: device under test.

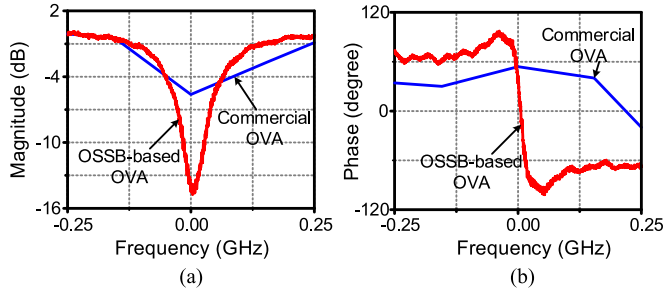


Fig. 2. The (a) magnitude and (b) phase responses of a phase-shifted FBG measured by the OSSB-based OVA and a typical commercial OVA based on the interferometry approach.

can be measured, since the nonlinear effects in the nonlinear devices would distort significantly the power spectral density of the OFDM signal, making the measurement inaccurate.

The other one is implemented based on optical single sideband (OSSB) modulation [25]–[33], which can potentially achieve sub-Hz resolution and large dynamic range. Fig. 1 shows the block diagram of the OSSB-based OVA. An optical carrier from a laser source is modulated by a RF signal at an OSSB modulator. The generated OSSB signal is propagating through the DUT, in which the magnitude and phase of the optical carrier and the sideband in the OSSB signal are changed according to the spectral responses of the DUT. Beating the two optical components at an optical-to-electrical conversion module, a photocurrent, carrying the spectral responses of the DUT, is obtained. Then, an electrical phase-magnitude detector referred by the RF signal is used to extract the magnitude and phase of the photocurrent, by which the magnitude and phase responses of the DUT at the wavelength of the optical sideband are achieved. Sweeping the frequency of the RF signal, the wavelength of the optical sideband is swept, so the optical spectral responses of the DUT at a certain wavelength range can be measured. Owing to the ultrahigh resolution of the frequency-swept RF source and the electrical phase-magnitude detector, the OSSB-based OVA can measure the spectral responses of optical devices with sub-Hz resolution in theory [26]. Previous experiment has reported a resolution of 78 kHz [27], which is much higher than the typical commercial OVA (LUNA OVA5000) based on the interferometry approach, as show in Fig. 2. Since only the optical carrier and one optical sideband exist in the optical DUT and only

the fundamental frequency component is detected by the electrical phase-magnitude detector, the OSSB-based OVA is able to measure the linear responses of optical devices with strong nonlinearity. In addition, the polarization responses can also be measured if the following changes are performed [28]–[33]: 1) adding a polarization controlling module before the DUT which can switch the polarization direction of the OSSB signal between two orthogonal polarization states, 2) implementing polarization diversity receiver in the optical-to-electrical conversion module, 3) performing two measurements using the OSSB signals with the two orthogonal polarization states.

Although the OSSB-based OVA is attractive because of its potential ultrahigh resolution, electrical-to-optical and optical-to-electrical conversions are required to achieve the electrical frequency sweeping and to detect the phase and magnitude information in the electrical domain, which introduces at least three key challenges. First, the measurement range is relatively small, typically less than 40 GHz (i.e. 0.32 nm in the 1550-nm band), limited mainly by the electrical bandwidth of the OSSB modulator, the photodetector (PD) and the phase-magnitude detector. Second, the nonlinearity in the EOMs would inevitably generate many unwanted high-order sidebands, leading to considerable measurement errors especially when the modulation index is large. In addition, the dynamic range of the OSSB-based OVA will be restricted by the limited sideband suppression ratio (SSR) of the practical OSSB signal. The recent progresses in solving the problems on measurement range and accuracy were briefly discussed in [25].

In this paper, the techniques developed in the past decade for improving the spectral measurement range, accuracy and dynamic range of the OSSB-based OVAs are discussed in more detail. Possible future research directions are also discussed.

II. PRINCIPLE

One key component in the OSSB-based OVA is the OSSB modulator, which can be implemented by a dual-drive EOM or two cascaded EOMs together with a 90° electrical hybrid coupler [34], [35], an optical filter to remove one of the two sidebands produced by a double-sideband modulator [27], [36], a dual-drive EOM with a 120° electrical hybrid coupler [37], and a double-sideband modulator followed by an optical Hilbert transformer [38]. Different modulation schemes would produce OSSB signals with different frequency components. To be general, we denote the OSSB signal as

$$E_{in}(\omega) = \sum_{n=-\infty}^{+\infty} A_n \cdot \delta[\omega - (\omega_o + n\omega_e)] \quad (1)$$

where ω_o and ω_e are the angular frequencies of the optical carrier and the RF signal, respectively, and A_n is the complex amplitude of the n th-order sideband. For example, an ideal OSSB signal contains only an optical carrier and one first-order sideband, so $A_0 \neq 0$ and $A_{+1} \neq 0$ (or $A_{-1} \neq 0$) while others equal to 0.

When the OSSB signal expressed in (1) goes through a DUT, the magnitude and phase of the carrier and sidebands are changed according to the transmission response of the DUT. At the output port of the DUT, the optical signal carrying the

spectral responses can be written as

$$E_{\text{out}}(\omega) = H(\omega) \cdot E_{\text{in}}(\omega) = \sum_{n=-\infty}^{+\infty} H(\omega_o + n\omega_e) \times A_n \cdot \delta[\omega - (\omega_o + n\omega_e)] \quad (2)$$

where $H(\omega) = H_{\text{DUT}}(\omega) \cdot H_{\text{sys}}(\omega)$, $H_{\text{DUT}}(\omega)$ and $H_{\text{sys}}(\omega)$ are the transmission responses of the DUT and the measurement system, respectively. After square-law detection in a PD, the optical signal is converted into a photocurrent. Given that the phase-magnitude detector only receives the frequency component which has the same frequency as the reference RF signal, only the ω_e -component in the photocurrent is detected, which can be expressed as

$$i(\omega_e) = \eta A_{+1} A_0^* H(\omega_o + \omega_e) H^*(\omega_o) + \eta A_0 A_{-1}^* H(\omega_o) \times H^*(\omega_o - \omega_e) + \eta \sum_{\substack{n=-\infty \\ n \neq -1, 0}}^{+\infty} A_{n+1} A_n^* \times H[\omega_o + (n+1)\omega_e] H^*(\omega_o + n\omega_e) \quad (3)$$

where η is the responsivity of the PD. In writing (3), we assume +1st-order sideband is the desired sideband of the OSSB signal. At the right hand of (3), the first term carries the actual spectral responses of the DUT, the second term represents the component beat by the optical carrier and the residual -1st-order sideband, and the third term denotes the beat notes of all the neighboring high-order sidebands.

If the OSSB signal is ideal, (3) can be simplified to

$$i(\omega_e) = \eta A_{+1} A_0^* H(\omega_o + \omega_e) H^*(\omega_o) \quad (4)$$

Let $H_{\text{DUT}}(\omega) = 1$, which can be implemented by removing the DUT and directly connecting two test ports, $H_{\text{sys}}(\omega)$ can be obtained,

$$i_{\text{sys}}(\omega_e) = \eta A_{+1} A_0^* H_{\text{sys}}(\omega_o + \omega_e) H_{\text{sys}}^*(\omega_o) \quad (5)$$

From (4) and (5), we can achieve the transmission response of the DUT by

$$H_{\text{DUT}}(\omega_o + \omega_e) = \frac{i(\omega_e)}{i_{\text{sys}}(\omega_e) H_{\text{DUT}}^*(\omega_o)} \quad (6)$$

where $H_{\text{DUT}}(\omega_o)$ is the spectral response of the DUT at ω_o , which can be seen as a complex constant.

The resolution of the OSSB-based OVA is mainly determined by the frequency tuning step of the RF source, the resolution of the electrical spectral analysis, and the linewidth of the laser source. To date, the RF source frequency tuning step and the electrical spectral analysis resolution can reach 0.1 Hz, and the linewidth of the laser source can be smaller than 0.1 Hz [39]. Therefore, the resolution of the OSSB-based OVA can reach 0.1 Hz in theory.

In practice, however, the ideal OSSB signal is very difficult to be generated. If the modulation index is large which is always the case to maintain a large signal-to-noise ratio of the optical microwave signal, the nonlinearity in the EOMs would inevitably generate unwanted high-order sidebands. These high-order sidebands would result in additional ω_e -component in the

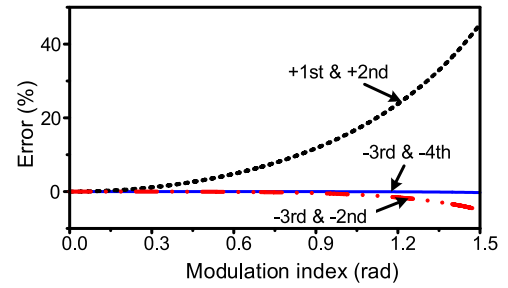


Fig. 3. The measurement errors induced by the beat notes of two neighboring high-order sidebands.

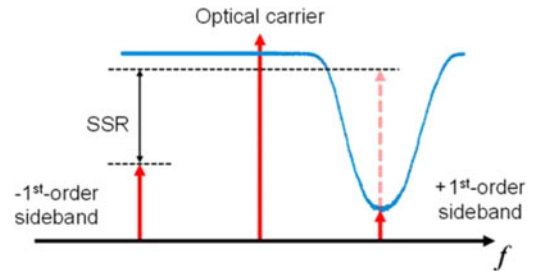


Fig. 4. The influence of the residual -1st-order sideband on the measurement accuracy.

photocurrent, which is presented in (3) as the third term at the right hand. Obviously, the measurement accuracy would be affected by these high-order sidebands [40]. For example, let $H_{\text{DUT}}(\omega) = 1$ we can calculate from (3) the measurement errors induced by the beat notes of any two neighboring high-order sidebands. Among these beat notes, the component beat by the +1st- and +2nd-order sidebands introduces the major errors because the powers of the +1st- and +2nd-order sidebands are generally larger than other high-order sidebands. It is worth noting that the measurement errors increase with the modulation index. When the modulation index is $\pi/3$, the +2nd-order-sideband-induced measurement error reaches 16.7%, which could significantly distort the measurement results.

Although the SSR, which is defined as the power ratio of the desired +1st-order sideband to the unwanted -1st-order sideband, of the OSSB signal can be as large as 40 dB [25]–[28], the residual -1st-order sideband could still cause measurement error. As can be seen from Fig. 4, when measuring deep notches, the power of the residual -1st-order sideband would be comparable or even higher than the notch-suppressed +1st-order sideband. Then, the second term at the right hand of (3) would be non-ignorable. Fig. 5 shows the magnitude and phase responses of a FBG achieved by the OSSB-based OVA using OSSB signals with different SSRs via numerical simulation. As can be seen, with the increase of the SSR, the measured magnitude response as well as the phase response approaches the actual responses. Therefore, the SSR of the OSSB signal is directly related to the dynamic range of the OSSB-based OVA. It is worth mentioning that the high-order sidebands would also affect the dynamic range especially when the modulation index of the OSSB modulator is large.

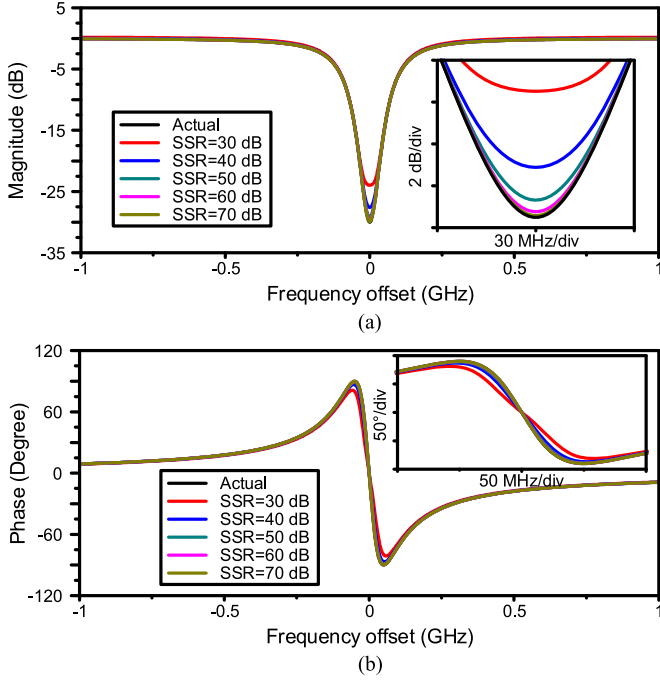


Fig. 5. The (a) magnitude and (b) phase responses achieved by the OSSB-based OVA using OSSB signals with different SSRs via numerical simulation.

III. BROADEN THE MEASUREMENT RANGE

One key problem associated with the OSSB-based OVA is its small measurement range which is restricted by the bandwidth of the EOMs, PDs and microwave devices. Typically, the measurement range of the OSSB-based OVA is less than 40 GHz, which cannot completely characterize the optical devices in hundreds or even thousands GHz range. Although a large measurement range can be achieved by turning the wavelength of a tunable laser source (TLS), the resolution would be greatly deteriorated due to the low wavelength accuracy and poor wavelength stability of the TLS (usually hundreds of MHz).

To extend the measurement range without deteriorating the measurement resolution, an OSSB-based OVA using an optical frequency comb (OFC) as the laser source was proposed [41]. In the OFC-based OVA, the interested frequency range is divided into several consecutive channels and the OFC with abundant comb lines provides the optical carriers for these channels. Then, a single-channel OSSB-based OVA is used to measure the spectral response in each channel one by one. By stitching the measured spectral responses together, the spectral responses of the DUT in the entire interested frequency range can be obtained. Benefitting from the fixed frequency spacing of the OFC, the measured spectral response can be precisely stitched together without deteriorating the measurement resolution.

Using the OFC-based OVA, the spectral responses in a range of $(n - 1) \times \Delta\omega + \Delta\omega_e$ can be measured if an OFC with n comb lines is employed, where $\Delta\omega$ and $\Delta\omega_e$ are the frequency spacing of the OFC and the measurement range of the single-channel OSSB-based OVA, respectively. $\Delta\omega$ must be smaller than or equal to $\Delta\omega_e$, so that the measured responses in the

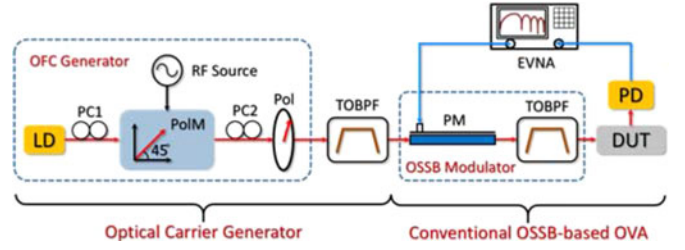


Fig. 6. Schematic diagram of the OSSB-based OVA using an OFC as the laser source. LD, laser diode; PC, polarization controller; PoIM, polarization modulator; Pol, polarizer; TOBPF, tunable optical bandpass filter; PM, phase modulator; RF, radio frequency; DUT, device under test; PD, photodetector; EVNA, electric vector network analyzer.

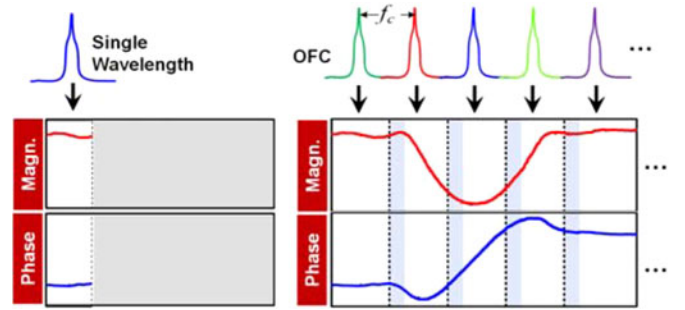


Fig. 7. Measurement range broadening using an OFC.

two neighboring channels can be stitched. Since the wavelength range of the frequency combs can cover C-band [42], the OSSB-based OVA using an OFC as the laser source has the capability of characterizing the optical devices over the whole C-band.

Fig. 6 shows the experiment setup of the OSSB-based OVA using an OFC as the laser source. The measurement system consists of two key parts, i.e. an OFC-based optical carrier generator and a conventional single-channel OSSB-based OVA. In the OFC-based optical carrier generator, a 5-comb-line OFC with a frequency spacing of 20 GHz is generated by a polarization modulator (PoIM) together with a polarizer [43]. A tunable optical bandpass filter (TOBPF) is followed to select one comb line from the OFC. The selected comb line serves as the optical carrier for the single-channel OSSB-based OVA to measure the spectral response of the DUT in the corresponding channel. Stitching the spectral responses of the DUT in all the five channels together, the spectral responses in a 105-GHz frequency range are obtained.

Fig. 7 shows the magnitude and phase responses of a FBG in a frequency range of 105 GHz measured by the OSSB-based OVA using an OFC as the laser source. In each channel, the measurement resolution is 1 MHz and the measurement range is 25 GHz (10~35 GHz away from the optical carrier). As compared with the 20-GHz frequency spacing of the OFC, there are 5-GHz frequency overlapped areas between every two neighboring channels (the shadows in Fig. 7). In these overlapped area, the measured spectral responses are well superimposed due to the fixed frequency spacing of the optical carriers. Hence, the measured responses in adjacent channels are precisely stitched

without deteriorating the measurement resolution and wideband spectral-response measurement are realized.

It should be noted that measuring wideband spectral responses of optical devices with an ultrahigh resolution is time consuming. In practice, the typical measurement speed of an OSSB-based OVA is 12.5 s/nm for a 100-kHz resolution, determined mainly by the scanning speed of the frequency swept RF source. When this speed is applied for the measurement of the spectral responses in the whole C-band (1530–1560 nm), the measurement time is more than 6 minutes. To speed up the measurement, a parallel measurement system based on dense wavelength-division multiplexing technology can be employed. The comb lines from the OFC are modulated by an OSSB modulator at the same time. The OSSB signals are propagating through the DUT and then separated by a dense wavelength-division multiplexer whose channel spacing equals to the frequency spacing of the OFC. In each channel, the magnitude and phase differences between the optical carrier and sideband are detected by a PD and a magnitude-phase detector. By scanning the frequency of the RF signal, the spectral responses in all channels are measured simultaneously. In this case, the spectral responses with a 100-kHz resolution in the whole C-band can be obtained in 2.5 second if an OFC with 25-GHz frequency spacing [42] is applied.

There are also other approaches to extend the measurement range [44]–[46], but the measurement range can only be increased by two or three times.

IV. SUPPRESS HIGH-ORDER-SIDEBAND INDUCED ERRORS

Due to the nonlinearity in EOMs, an OSSB signal in reality always comprises of many high-order sidebands (i.e. $\pm 2\text{nd-}$, $\pm 3\text{rd-}$, \dots , $\pm \text{nth-}$ order sidebands). Analytical analysis and numerical simulation have been performed to investigate the influence of these high-order sidebands on the accuracy of the measured responses [40], showing that considerable measurement errors are presented if the modulation index of the EOM is large. Applying small modulation index can undoubtedly reduce the high-order-sideband induced errors, but it also leads to large noise in the measured responses since the desired $+1\text{st-}$ order sideband is also small.

According to [40], the $+2\text{nd-}$ order sideband would introduce the largest errors due to its high power. Therefore, one approach to reduce the high-order-sideband induced errors is to suppress the $+2\text{nd-}$ order sideband. To do so, an OSSB modulation method based on a 120° electrical hybrid coupler and a dual-drive Mach-Zehnder modulator was proposed, which can simultaneously suppress the -1st- and $+2\text{nd-}$ order sidebands [37]. Fig. 8 shows the optical spectrum of the experimentally generated OSSB signals based on the 120° electrical hybrid coupler when the modulation index is 1.92. As a comparison, the optical spectrum of the OSSB signal generated by a conventional 90° degree electrical hybrid coupler and a dual-drive Mach-Zehnder modulator is also plotted. As can be seen, the $+2\text{nd-}$ order sideband is suppressed by 23.87 dB. Then, the OSSB signals with the $+2\text{nd-}$ order sideband suppressed is applied in the OSSB-based OVA to characterize the spectral responses of a FBG. Fig.

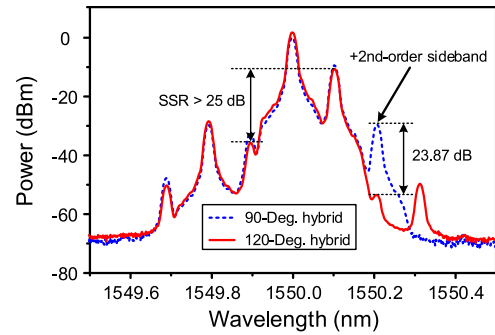


Fig. 8. The optical spectra of the OSSB signals generated by the OSSB modulation schemes based on (a) a 90° electrical hybrid coupler and (b) a 120° electrical hybrid coupler.

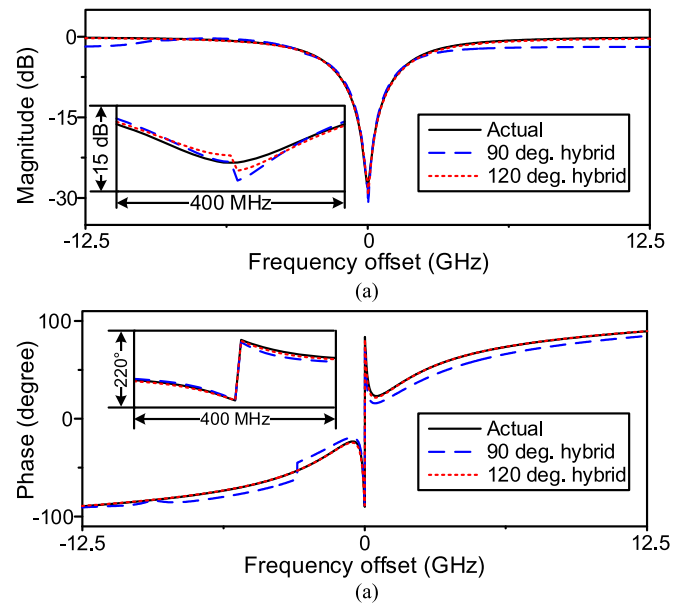


Fig. 9. The actual responses and the measured responses of a FBG in simulation when the phase modulation index is 1. (a) Magnitude responses, and (b) phase responses.

9 shows the magnitude and phase responses achieved by simulation. The responses obtained by the OVA adopting the 120° electrical hybrid coupler based OSSB modulation are almost coincided with the actual ones, while the OVA employing the conventional 90° electrical hybrid coupler based OSSB modulation achieves the responses together with large measurement errors.

If the modulation index further increases, the measurement errors introduced by other high-order sidebands become considerable, as can be seen from Fig. 3. To effectively remove these errors, an approach based on off-line error cancellation was proposed [47]. Three-step measurement is performed. In the first step, a RF-modulated OSSB signal with a high SSR is applied and a photocurrent is generated which is comprised by the component carrying the actual spectral responses of the DUT and the high-order-sideband induced measurement errors,

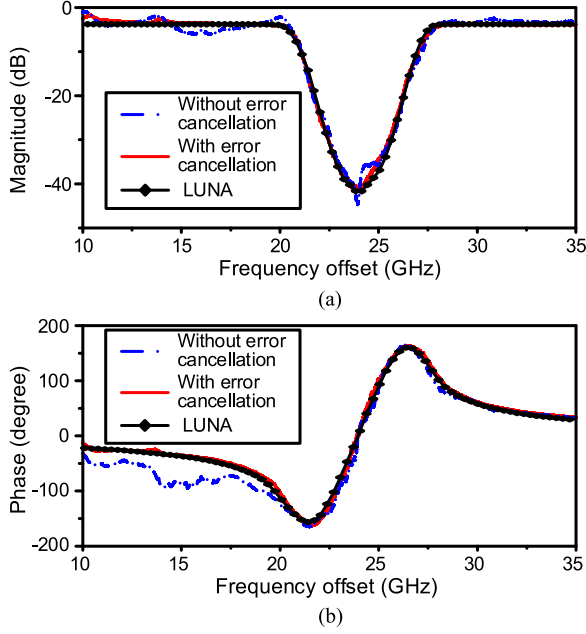


Fig. 10. The (a) magnitude and (b) phase responses of the FBG measured with and without error cancellation when the modulation index is 1.68 and a typical commercial OVA (LUNA OVA5000).

i.e.

$$i_{1st}(\omega_e) = \eta A_{+1} A_0^* H(\omega_o + \omega_e) H^*(\omega_o) + \eta \sum_{\substack{n=-\infty \\ n \neq -1, 0}}^{+\infty} A_{n+1} \\ \times A_n^* H[\omega_o + (n+1)\omega_e] H^*(\omega_o + n\omega_e) \quad (7)$$

Then, removing the optical carrier from the OSSB signal and performing a second measurement. In this case, the photocurrent is exactly the measurement errors introduced by the high-order sidebands, given by

$$i_{2nd}(\omega_e) = \eta \sum_{\substack{n=-\infty \\ n \neq -1, 0}}^{+\infty} A_{n+1} A_n^* H[\omega_o + (n+1)\omega_e] \\ \times H^*(\omega_o + n\omega_e) \quad (8)$$

Subtracting the measured result in the second measurement from the first one, the measurement errors introduced by the high-order sidebands are fully eliminated. By detecting the magnitude and phase in the electrical domain, the actual spectral responses of the DUT are achieved.

Fig. 10 shows the magnitude and phase responses of a FBG measured by the OSSB-based OVA with and without error cancellation, when the modulation index is 1.68. As can be seen, the responses measured by the conventional OSSB-based OVA contain large measurement errors. Eliminating the high-order-sideband induced errors by the three-step measurement, the accurate spectral responses are achieved, which agree well with those measured by a commercial OVA (LUNA OVA5000). In [48], the absorption spectrum of stimulated Brillouin scattering in optical fibers is used to replace the optical filter in [47], to

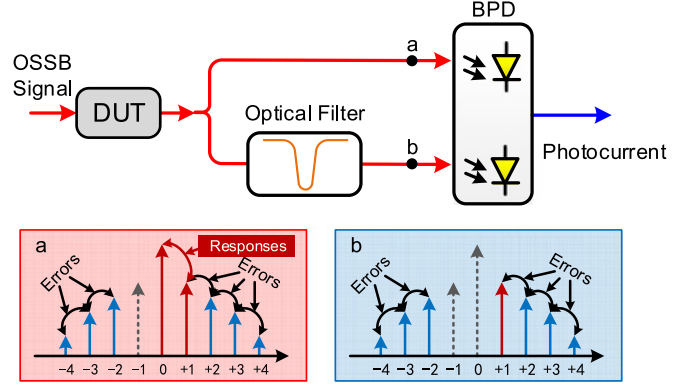


Fig. 11. OSSB-based OVA employing balanced photodetection.

manipulate the optical carrier in the OSSB signal, which also achieves the error cancellation.

It should be noted that in [47], [48] adjustment of the optical filter is required between the two measurements, which not only increases the measurement time but also introduces additional measurement error if the center wavelength of the optical filter is not accurately controlled. To solve this problem, a modified approach employing a balanced photodetector (BPD) was developed [49]. The schematic diagram is shown in Fig. 11. The OSSB signal after the DUT is divided into two parts. One part is directly sent to one optical port of the BPD, and the other part is directed to the other optical port of the BPD after suppressing the optical carrier. The two optical signals are simultaneously converted into photocurrents and vectorially subtracted at the output port of the BPD. According to the analytical model, the detection of the OSSB signal with the optical carrier results in a photocurrent containing the actual responses and the high-order-sideband induced errors, while the carrier-suppressed OSSB signal generates a photocurrent consisting only the high-order-sideband induced errors. As a result, the output photocurrent of the BPD carries the accurate responses of the DUT. Fig. 12 shows the magnitude and phase responses measured by the conventional OSSB-based OVA and the OSSB-based OVA with balanced photodetection when the modulation index of the OSSB modulator is 2.81. As can be seen, the responses measured by the conventional OVA are obviously deviated from the actual ones due to the large measurement errors. By employing the balanced photodetection, the high-order-sideband induced errors are significantly suppressed. The magnitude and phase responses measured by LUNA OVA5000 are also plotted for comparison, which are coincided with those measured by the OVA using balanced photodetection. It should be noted that the signal-to-noise ratio of the spectral responses is also improved since the BPD can effectively suppress the common-mode noise in the measurement system.

Theoretically, the measurement errors induced by the high-order sidebands can be completely suppressed. However, the finite common-mode rejection ratio (CMRR) of a practical measurement system, which is seriously affected by the temperature variation and the imbalanced responsivity of the BPD, would eventually limit the system performance. Fig. 13 shows the

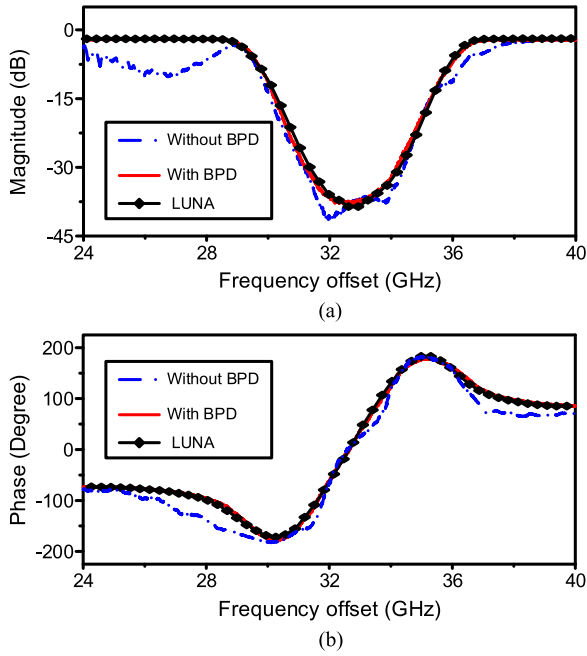


Fig. 12. The (a) magnitude and (b) phase responses of the FBG measured by the conventional OSSB-based OVA and the OSSB-based OVA with balanced photodetection.

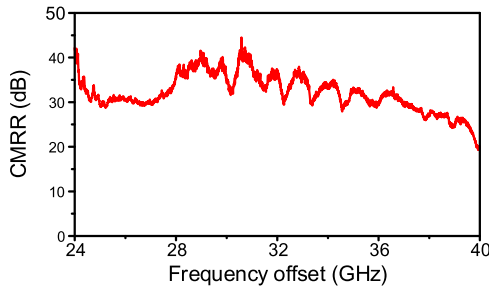


Fig. 13. The measured CMRR of the OSSB-based OVA employing balanced photodetection.

CMRR measured by introducing two identical signals into the BPD after carefully adjusting the length and IL of the two paths. As can be seen, the CMRR of the measurement system is about 30 dB, indicating that the high-order-sideband induced errors and common-mode noise can be suppressed by about 30 dB.

By removing the measurement errors induced by the high-order sidebands, large modulation index of the OSSB modulator can be applied, which can increase the capability of the OSSB-based OVA for measuring very small spectral responses. Fig. 14 shows the measured magnitude responses at the bottom of an FBG's notch with different modulation indices. As can be seen, the signal-to-noise ratio increases with the modulation index.

V. IMPROVE DYNAMIC RANGE

Dynamic range is one of the most important parameters for practical spectral-response measurement. Because the optical power is concentrated on a single-frequency component, the OSSB-based OVA would have a much larger dynamic range

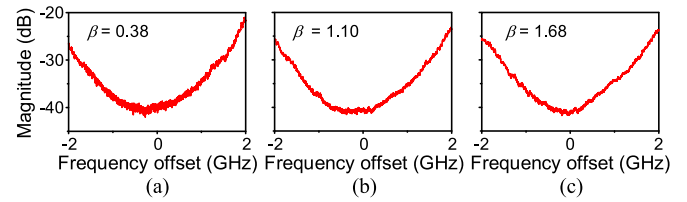


Fig. 14. The measured magnitude responses at the bottom of an FBG's notch when the modulation indices are (a) 0.38, (b) 1.10 and (c) 1.68, respectively.

than the OCE-based OVA [22]. However, the SSR of the swept OSSB signal would place a restriction on the further increase of the dynamic range, as can be seen from Fig. 4. Typically, the SSR of a wideband-swept OSSB signal is less than 40 dB, so the responses of the bandstop devices with deep notch cannot be accurately measured.

To improve the dynamic range, an effective way is to perform the measurement twice using two OSSB signals with different SSRs [50]. Assuming the modulation index of the OSSB modulator is small so that the high-order sidebands can be ignored, (3) can be simplified to

$$i_1(\omega_e) = \eta A_{+1} A_0^* H(\omega_o + \omega_e) H^*(\omega_o) + \eta A_0 A_{-1}^* H(\omega_o) \times H^*(\omega_o - \omega_e) \quad (9)$$

$$i_2(\omega_e) = \eta \alpha A_{+1} A_0^* H(\omega_o + \omega_e) H^*(\omega_o) + \eta \beta A_0 A_{-1}^* \times H(\omega_o) H^*(\omega_o - \omega_e) \quad (10)$$

where α and β ($\alpha \neq \beta$) are two known coefficients to form different SSRs. With (9) and (10), the spectral responses of the DUT can be accurately calculated,

$$H_{\text{DUT}}(\omega_o + \omega_e) = \frac{\beta i_1(\omega_e) - i_2(\omega_e)}{(\beta - \alpha) i_{\text{sys}}(\omega_e) H_{\text{DUT}}^*(\omega_o)} \quad (11)$$

As a result, the influence of the undesired -1 st-order sideband is eliminated. In an experiment, the magnitude and phase responses of a phase-shifted fiber Bragg grating are measured when the SSR of the OSSB signal is 10, 20 and 40 dB, respectively. Referring the magnitude response measured by the OSSB signal with a SSR of 40 dB, the measurement errors are 8.1 and 1.9 dB for the cases using 10- and 20-dB SSRs, showing that the dynamic range increases with the SSR. Then, taking the currents measured by the OSSB signals with SSRs of 10 and 20 dB into (11), the accurate magnitude and phase responses are calculated, which agree well with those measured by the OSSB signal with a SSR of 40 dB. This approach, however, is only effective when the modulation index of the OSSB modulator is small since only the optical carrier and two first-order sidebands are considered. If the high-order sidebands are taken into account, the accurate spectral responses cannot be calculated. In addition, a change of the modulation scheme between the two measurements is required, which not only increases the measurement time but also introduces additional measurement error since the SSR of an OSSB signal is always difficult to be accurately controlled.

To increase the dynamic range of the OSSB-based OVA without premise on the modulation index of the OSSB modulator, an approach based on optical Hilbert transform and balanced photodetection was recently proposed [51], which can suppress the error induced by the residual unwanted first-order sideband together with the high-order sideband induced errors. In the scheme, the OSSB signal after the DUT is split into two portions. One portion is directly introduced to one optical port of the BPD, which can be expressed as

$$\begin{aligned}
 E_U(\omega) = & A_{-1} \cdot \delta[\omega - (\omega_o - \omega_e)] + A_0 \cdot \delta(\omega - \omega_o) \\
 & + A_{+1} \cdot \delta[\omega - (\omega_o + \omega_e)] + \sum_{n=-2}^{+\infty} A_n \cdot \delta \\
 & \times [\omega - (\omega_o + n\omega_e)] + \sum_{n=2}^{+\infty} A_n \cdot \delta \\
 & \times [\omega - (\omega_o + n\omega_e)] \quad (12)
 \end{aligned}$$

where A_n is the complex amplitude of the n th-order sideband. The other portion is sent to the other optical port of the BPD after propagating through an optical Hilbert transformer. In the optical Hilbert transformer, the phase of the positive sidebands are reversed, so the signal can be written as

$$\begin{aligned}
 E_L(\omega) = & A_{-1} \cdot \delta[\omega - (\omega_o - \omega_e)] + A_0 \cdot \delta(\omega - \omega_o) \\
 & - A_{+1} \cdot \delta[\omega - (\omega_o + \omega_e)] + \sum_{n=-2}^{+\infty} A_n \cdot \delta \\
 & \times [\omega - (\omega_o + n\omega_e)] - \sum_{n=2}^{+\infty} A_n \cdot \delta \\
 & \times [\omega - (\omega_o + n\omega_e)] \quad (13)
 \end{aligned}$$

In the BPD, two photocurrents are generated, given by

$$\begin{aligned}
 i_U(\omega_e) = & \eta A_0 A_{-1}^* H(\omega_o) H^*(\omega_o - \omega_e) + \eta A_{+1} A_0^* \\
 & \times H(\omega_o + \omega_e) H^*(\omega_o) + \eta \sum_{\substack{n=-\infty \\ n \neq -1, 0}}^{\infty} A_{n+1} A_n^* \\
 & \times H[\omega_o + (n+1)\omega_e] H^*(\omega_o + n\omega_e) \quad (14)
 \end{aligned}$$

$$\begin{aligned}
 i_L(\omega_e) = & \eta A_0 A_{-1}^* H(\omega_o) H^*(\omega_o - \omega_e) - \eta A_{+1} A_0^* \\
 & \times H(\omega_o + \omega_e) H^*(\omega_o) + \eta \sum_{\substack{n=-\infty \\ n \neq -1, 0}}^{\infty} A_{n+1} A_n^* \\
 & \times H[\omega_o + (n+1)\omega_e] H^*(\omega_o + n\omega_e) \quad (15)
 \end{aligned}$$

At the right hand of (14) and (15), the first and third terms are the measurement errors induced by the residual -1 st-order sideband and the high-order sidebands, which are in phase. The second terms carrying the transmission responses of the DUT are out of phase. At the output port of the BPD, the two photocurrents are vectorially subtracted. Thereby, both the residual -1 st-order-sideband-induced measurement error and the high-order-sideband-induced measurement errors are suppressed and

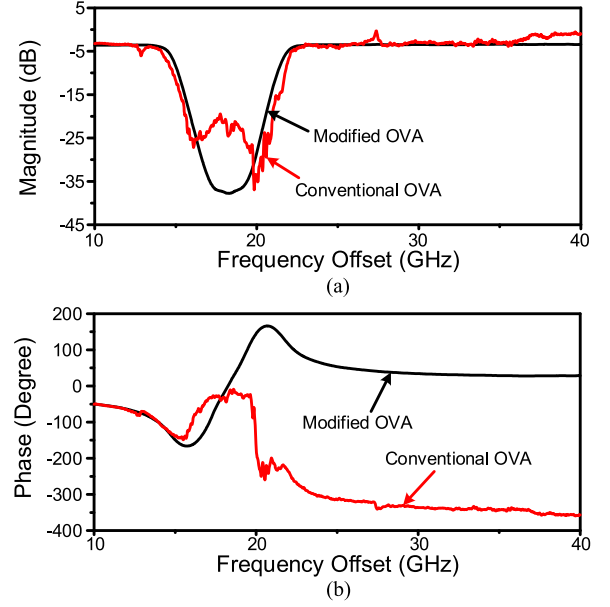


Fig. 15. The (a) magnitude and (b) phase responses measured by the conventional OVA and the OVA based on optical Hilbert transform and balanced photodetection.

the output photocurrent only contains the component beat by the optical carrier and the $+1$ st-order sideband.

Fig. 15 shows the magnitude and phase responses of a FBG (TeraXion Inc.) measured by the conventional OVA using the OSSB modulation based on a 90° electrical hybrid coupler and a dual-drive MZM. The OSSB signal has a SSR of less than 20 dB which is much smaller than the notch depth of the FBG. Because of the uneven frequency response of the 90° electrical hybrid coupler and the undesirable-sideband-induced measurement errors, the measurement results are significantly distorted. When the approach based on optical Hilbert transform and balanced photodetection is applied, the measurement errors are significantly suppressed and accurate responses are achieved, indicating that the dynamic range is greatly improved.

It should be noted that the improvement of the dynamic range could not be infinity due to the imbalance of the responsivity of the PDs in the BPD. Since the CMRR of the BPD is larger than 30 dB, the measurement errors and common mode noise can be greatly suppressed and at least 30-dB dynamic range improvement can be achieved.

VI. CONCLUSION AND DISCUSSION

In conclusion, an OSSB-based OVA can achieve exceptional high measurement resolution, but its small measurement range, large measurement errors induced by high-order sidebands and relatively small dynamic range restricted by the SSR of the OSSB signal prohibit it from gaining ground in optics and photonics. To broaden the measurement range, an OFC can be used to provide optical carriers with fixed frequency spacing for channel by channel measurement; to suppress the high-order-sideband-induced measurement errors, carrier suppression together with balanced photodetection can be applied; and to increase the measurement dynamic range, balanced photodetection and optical Hilbert transform is effective.

Although the performance of the OSSB-based OVA has been greatly improved in the past decade, the maturity level of the technique can still be improved in the following aspects. First, system architecture to reduce the cost is highly desired because both of the wideband frequency-swept RF source and the high-frequency phase-magnitude detector are expensive. One possible way to reduce the cost is to apply photonic microwave mixing [52] so a low-frequency phase-magnitude detector can extract the phase and magnitude information. Second, the current solutions to improve the measurement accuracy and dynamic range are wavelength dependent because of the use of narrowband optical filters. This will increase significantly the operation complexity especially when broadband measurement is required, so high performance OSSB-based OVA without the use of the optical filter is welcomed. Last but not least, most of the OSSB-based OVAs are operated in the 1550-nm band thanks to the mature laser sources, modulators and detectors in this band. However, many applications requiring high-Q optical devices, such as the label-free biosensing, single-molecule detection, and optical metrology, are operated in other bands. Therefore, considerable efforts should be devoted to the development of OSSB-based OVAs in new wavelength bands.

REFERENCES

- [1] F. Vollmer and S. Arnold, "Whispering-gallery-mode biosensing: label-free detection down to single molecules," *Nature Methods*, vol. 5, pp. 591–596, 2008.
- [2] A. Yalcin *et al.*, "Optical sensing of biomolecules using microring resonators," *IEEE J. Sel. Topics Quantum Electron.*, vol. 12, no. 1, pp. 148–155, Jan./Feb. 2006.
- [3] M. D. Baaske, M. R. Foreman, and F. Vollmer, "Single-molecule nucleic acid interactions monitored on a label-free microcavity biosensor platform," *Nature Nanotech.*, vol. 9, no. 11, pp. 933–939, 2014.
- [4] L. Chang *et al.*, "Parity-time symmetry and variable optical isolation in active-passive-coupled microresonators," *Nature Photon.*, vol. 8, no. 7, pp. 524–529, 2014.
- [5] L. Liu *et al.*, "An ultra-small, low-power, all-optical flip-flop memory on a silicon chip," *Nature Photon.*, vol. 4, no. 3, pp. 182–187, 2010.
- [6] E. Karimi and R. W. Boyd, "Ten years of nature physics: slowly but surely," *Nature Phys.*, vol. 11, no. 1, pp. 15–16, 2015.
- [7] W. S. Fegadolli *et al.*, "Experimental demonstration of a reconfigurable silicon thermo-optical device based on spectral tuning of ring resonators for optical signal processing," *Opt. Exp.*, vol. 22, no. 3, pp. 3425–3431, 2014.
- [8] D. J. Moss, R. Morandotti, A. L. Gaeta, and M. Lipson, "New CMOS-compatible platforms based on silicon nitride and Hydex for nonlinear optics," *Nature Photon.*, vol. 7, no. 8, pp. 597–607, 2013.
- [9] T. Nacke, A. Barthel, D. Frense, M. Meister, and B. P. Cahill, "Application of high frequency sensors for contactless monitoring in disposable bioreactors," *Chemie Ingenieur Technik*, vol. 85, nos. 1/2, pp. 179–185, 2013.
- [10] X. Wang *et al.*, "Suspended ultra-small disk resonator on silicon for optical sensing," *Opt. Lett.*, vol. 38, no. 24, pp. 5405–5408, 2013.
- [11] Y. Painchaud, M. Aubé, G. Brochu, and M.-J. Picard, "Ultra-narrowband notch filtering with highly resonant fiber Bragg gratings," presented at the *Bragg Gratings, Photosensitivity, Poling Glass Waveguides, OSA Tech. Dig.*, 2010, Paper BTuC3.
- [12] A. A. Savchenkov, V. S. Ilchenko, A. B. Matsko, and L. Maleki, "Kilohertz optical resonances in dielectric crystal cavities," *Phys. Rev. A*, vol. 70, p. 051804, 2004.
- [13] T. Niemi, M. Uusimaa, and H. Ludvigsen, "Limitations of phase-shift method in measuring dense group delay ripple of fiber Bragg gratings," *IEEE Photon. Technol. Lett.*, vol. 13, no. 12, pp. 1334–1336, Dec. 2001.
- [14] D. K. Gifford, B. J. Soller, M. S. Wolfe, and M. E. Froggatt, "Optical vector network analyzer for single-scan measurements of loss, group delay, and polarization mode dispersion," *Appl. Opt.*, vol. 44, no. 34, pp. 7282–7286, 2005.
- [15] <http://lunainc.com/OVA5000>, 2016.
- [16] B. Szafraniec and D. M. Baney, "Elementary matrix-based vector optical network analysis," *J. Lightw. Technol.*, vol. 25, no. 4, pp. 1061–1069, Apr. 2007.
- [17] D. M. Baney and B. Szafraniec, "Elementary matrix method for dispersion analysis in optical systems," *J. Lightw. Technol.*, vol. 28, no. 4, pp. 294–307, Feb. 15, 2010.
- [18] X. W. Yi, W. Shieh, and Y. Ma, "Phase noise effects on high spectral efficiency coherent optical OFDM transmission," *J. Lightw. Technol.*, vol. 26, no. 10, pp. 1309–1316, May 15, 2008.
- [19] W. Shieh, R. S. Tucker, W. Chen, X. W. Yi, and G. Pendock, "Optical performance monitoring in coherent optical OFDM systems," *Opt. Exp.*, vol. 15, no. 2, pp. 350–356, 2007.
- [20] F. N. Hauske, M. Kuschnerov, B. Spinnler, and B. Lankl, "Optical performance monitoring in digital coherent receivers," *J. Lightw. Technol.*, vol. 27, no. 16, pp. 3623–3631, Aug. 15, 2009.
- [21] M. S. Faruk, Y. Mori, C. Zhang, K. Igarashi, and K. Kikuchi, "Multi-impairment monitoring from adaptive finite-impulse-response filters in a digital coherent receiver," *Opt. Exp.*, vol. 18, no. 26, pp. 26929–26936, 2010.
- [22] X. W. Yi, Z. H. Li, Y. Bao, and Q. K. Qiu, "Characterization of passive optical components by DSP-based optical channel estimation," *IEEE Photon. Technol. Lett.*, vol. 24, no. 6, pp. 443–445, Mar. 15, 2012.
- [23] C. Jin *et al.*, "High-resolution optical spectrum characterization using optical channel estimation and spectrum stitching technique," *Opt. Lett.*, vol. 38, no. 13, pp. 2314–2316, 2013.
- [24] Z. H. Li and X. W. Yi, "Spectral characterization of passive optical devices," *Proc. SPIE Newsroom Sens. Meas.*, pp. 1–3, Feb. 18, 2014, Available: http://spie.org/documents/Newsroom/Imported/005331/005331_10.pdf
- [25] S. L. Pan and M. Xue, "Optical vector analysis with ultra-high resolution," presented at the *Opt. Fiber Commun. Conf.*, Anaheim, CA, USA, 2016, Paper W4K.1.
- [26] J. E. Román, M. Y. Frankel, and R. D. Esman, "Spectral characterization of fiber gratings with high resolution," *Opt. Lett.*, vol. 23, no. 12, pp. 939–941, 1998.
- [27] Z. Z. Tang, S. L. Pan, and J. P. Yao, "A high resolution optical vector network analyzer based on a wideband and wavelength-tunable optical single-sideband modulator," *Opt. Exp.*, vol. 20, no. 6, pp. 6555–6560, 2012.
- [28] A. Loayssa, R. Hernández, D. Benito, and S. Galech, "Characterization of stimulated Brillouin scattering spectra by use of optical single-sideband modulation," *Opt. Lett.*, vol. 29, no. 6, pp. 638–640, 2004.
- [29] R. Hernandez, A. Loayssa, and D. Benito, "Optical vector network analysis based on single-sideband modulation," *Opt. Eng.*, vol. 43, no. 10, pp. 2418–2421, Oct. 2004.
- [30] M. Sagues, G. Beloki, and A. Loayssa, "Broadband swept optical single-sideband modulation generation for spectral characterization of optical components," in *Proc. 33rd Eur. Conf. Exhib. Opt. Commun.*, 2007, pp. 1–2.
- [31] M. Sagues, M. Pérez, and A. Loayssa, "Measurement of polarization dependent loss, polarization mode dispersion and group delay of optical components using swept optical single sideband modulated signals," *Opt. Exp.*, vol. 16, no. 20, pp. 16181–16188, 2008.
- [32] M. Sagues and A. Loayssa, "Swept optical single sideband modulation for spectral measurement applications using stimulated Brillouin scattering," *Opt. Exp.*, vol. 18, no. 16, pp. 17555–17568, 2010.
- [33] M. Sagues and A. Loayssa, "Spectral characterisation of polarisation dependent loss of optical components using optical single sideband modulation," *Electron. Lett.*, vol. 47, no. 1, pp. 47–49, 2011.
- [34] G. H. Smith, D. Novak, and Z. Ahmed, "Overcoming chromatic-dispersion effects in fiber-wireless systems incorporating external modulators," *IEEE Trans. Microw. Theory Technol.*, vol. 45, no. 8, pp. 1410–1415, Aug. 1997.
- [35] Y. M. Zhang, F. Z. Zhang and S. L. Pan, "Optical single sideband modulation with tunable optical carrier-to-sideband ratio," *IEEE Photon. Technol. Lett.*, vol. 26, no. 7, pp. 653–655, Apr. 1, 2014.
- [36] S. R. Blais and J. P. Yao, "Optical single sideband modulation using an ultranarrow dual-transmission-band fiber Bragg grating," *IEEE Photon. Technol. Lett.*, vol. 18, no. 21, pp. 2230–2232, Nov. 1, 2006.
- [37] M. Xue, S. L. Pan, and Y. J. Zhao, "Optical single-sideband modulation based on a dual-drive MZM and a 120-degree hybrid coupler," *J. Lightw. Technol.*, vol. 32, no. 19, pp. 3317–3323, Oct. 1, 2014.

- [38] Z. Li, H. Chi, X. Zhang, and J. P. Yao, "Optical single-sideband modulation using a fiber-Bragg-grating-based optical Hilbert transformer," *IEEE Photon. Technol. Lett.*, vol. 23, no. 9, pp. 558–560, May 1, 2011.
- [39] T. Kessler *et al.*, "A sub-40-mHz-linewidth laser based on a silicon single-crystal optical cavity," *Nature Photon.*, vol. 6, no. 10, pp. 687–692, 2012.
- [40] M. Xue, S. L. Pan, X. W. Gu, and Y. J. Zhao, "Performance analysis of optical vector analyzer based on optical single-sideband modulation," *J. Opt. Soc. America B*, vol. 30, no. 4, pp. 928–933, 2013.
- [41] M. Xue, S. L. Pan, C. He, R. H. Guo, and Y. J. Zhao, "Wideband optical vector network analyzer based on optical single-sideband modulation and optical frequency comb," *Opt. Lett.*, vol. 38, no. 22, pp. 4900–4902, 2013. http://www.optocomb.com/files/8814/3591/2663/eng_wtas_02.pdf, 2015.
- [43] C. He, S. L. Pan, R. H. Guo, Y. J. Zhao, and M. H. Pan, "An ultra-flat optical frequency comb generated based on cascaded polarization modulators," *Opt. Lett.*, vol. 37, no. 18, pp. 3834–3836, 2012.
- [44] W. Li, W. T. Wang, L. X. Wang, and N. H. Zhu, "Optical vector network analyzer based on single-sideband modulation and segmental measurement," *IEEE Photon. J.*, vol. 6, no. 2, pp. 1–8, 2014.
- [45] T. Qing, M. Xue, M. H. Huang and S. L. Pan, "Measurement of optical magnitude response based on double-sideband modulation," *Opt. Lett.*, vol. 39, no. 21, pp. 6174–6176, 2014.
- [46] T. Qing, S. P. Li, M. Xue, and S. L. Pan, "Optical vector analysis based on double-sideband modulation and stimulated Brillouin scattering," *Opt. Lett.*, vol. 41, no. 15, pp. 3671–3674, 2016.
- [47] M. Xue, S. L. Pan, and Y. J. Zhao, "Accuracy improvement of optical vector network analyzer based on single-sideband modulation," *Opt. Lett.*, vol. 39, no. 12, pp. 3595–3598, 2014.
- [48] W. T. Wang *et al.*, "Optical vector network analyzer with improved accuracy based on Brillouin-assisted optical carrier processing," *IEEE Photon. J.*, vol. 6, no. 6, pp. 1–10, Apr. 2014.
- [49] M. Xue, S. L. Pan, and Y. J. Zhao, "Accurate optical vector network analyzer based on optical single-sideband modulation and balanced photodetection," *Opt. Lett.*, vol. 40, no. 4, pp. 569–572, 2015.
- [50] M. Wang and J. P. Yao, "Optical vector network analyzer based on unbalanced double-sideband modulation," *IEEE Photon. Technol. Lett.*, vol. 25, no. 8, pp. 753–755, Apr. 15, 2013.
- [51] M. Xue, S. L. Pan, and Y. J. Zhao, "Large dynamic range optical vector analyzer based on optical single-sideband modulation and Hilbert transform," *Appl. Phys. B: Laser Opt.*, vol. 122, no. 7, p. 197, Jul. 2016.
- [52] Z. Z. Tang and S. L. Pan, "A filter-free photonic microwave single sideband mixer," *IEEE Microw. Wireless Compon. Lett.*, vol. 26, no. 1, pp. 67–69, Jan. 2016.

Shilong Pan (S'06–M'09–SM'13) received the B.S. and Ph.D. degrees in electronics engineering from Tsinghua University, Beijing, China, in 2004 and 2008, respectively. From 2008 to 2010, he was a "Vision 2010" Postdoctoral Research Fellow in the Microwave Photonics Research Laboratory, University of Ottawa, Ottawa, ON, Canada. He joined the College of Electronic and Information Engineering, Nanjing University of Aeronautics and Astronautics, Nanjing, China, in 2010, where he is currently a Full Professor and an Executive Director of the Key Laboratory of Radar Imaging and Microwave Photonics (Nanjing Univ. Aeronaut. Astronaut.), Ministry of Education.

His research has focused on microwave photonics, which includes optical generation and processing of microwave signals, analog photonic links, photonic microwave measurement, and integrated microwave photonics. He has authored or coauthored over 250 research papers, including more than 130 papers in peer-reviewed journals and 120 papers in conference proceedings.

Dr. Pan is a Senior Member of the IEEE Microwave Theory and Techniques Society, the IEEE Photonics Society, the IEEE Instrumentation and Measurement Society, and a Member of the Optical Society of America. He was selected to receive an OSA Outstanding Reviewer Award in 2015. He serves as a Chair of numerous international conferences and workshops, including the TPC Chair of the International Conference on Optical Communications and Networks in 2015, TPC Chair of the high-speed and broadband wireless technologies subcommittee of the IEEE Radio Wireless Symposium in 2013, 2014, and 2016, TPC Chair of the Optical fiber sensors and microwave photonics subcommittee of the OptoElectronics and Communication Conference in 2015, and Chair of the microwave photonics for broadband measurement workshop of International Microwave Symposium in 2015.

Min Xue was born in Changzhou, China, in September 1988. He received the B.S. degree from the College of Electronic and Information Engineering, Nanjing University of Aeronautics and Astronautics, Nanjing, China, in 2011, where he is currently working toward the Ph.D. degree. His research interests include photonic microwave measurement and metrology, optical fiber sensor, and integrated microwave photonics.